

DNA phosphates are effective catalysts for asymmetric ion-pairing catalysis in water

In the format provided by the
authors and unedited

Table of Contents

Supplementary Methods	2
General Information	2
Optimization of Reaction Conditions	4
Preparation of Materials	6
Computational Methods	36
Characterization of Products	45
Copies of NMR spectra	274
Supplementary References	423

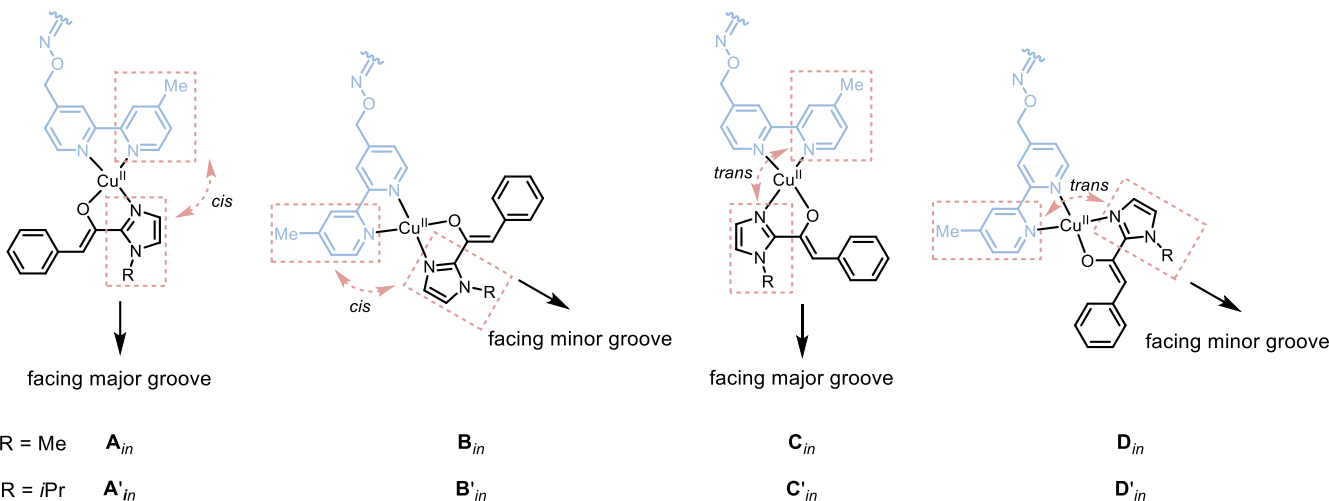
Computational Methods

Geometries of DNA-catalyst systems were optimized at GFN2-xTB4³⁻⁵ level of theory with *crude* optimization settings. We note that geometry optimizations did not always converge (i.e., converged for some systems but not others) for optimization settings of *vtight*, *tight*, *normal*, *lax*, *loose* and *sloppy*. Only *crude* optimization settings manage to have geometry optimization convergence for all systems.

The xTB-optimized structures were subject to single-point energy calculations using density function theory (DFT), which were performed using the *Gaussian 16* rev. B.01 program.⁶ Single point (SP) corrections were performed using BP86 functional^{7,8} with Grimme's D3 dispersion correction⁹ with Becke-Johnson damping¹⁰⁻¹³ (hereafter denoted BP86-D3BJ) with 6-311+G(d) basis set¹⁴ for all atoms. Dispersion correction (D3BJ) has been added to correctly capture non-covalent interactions.¹⁵⁻¹⁸ The implicit SMD continuum solvation model¹⁹ was used to account for the solvent effect of water that was used in the experimental reactions. The single point energies, calculated at SMD (water)-BP86-D3BJ/6-311+G(d) level of theory, are given in kcal mol⁻¹ and used for discussion throughout. All molecular structures and molecular orbitals were visualized using *PyMOL* software.²⁰

Naming conventions

Structures are named according to the figure below. Structures where the imidazole group and the 4-methylpyridine are in *cis* relationship will be either **A** or **B**, depending on which DNA groove it faces: if the bpy ligand N atoms face major groove, this will be **A** and if minor groove, **B**. Similarly, structures where the imidazole group and the 4-methylpyridine are in *trans* relationship will be either **C** or **D**, where in **C**, the bpy ligand N atoms face major groove and in **D**, the bpy ligand N atoms face minor groove. For fluorination reaction, unprimed labels (**A** to **D**) are used and for Mannich reaction, primed labels are used (**A'** to **D'**).

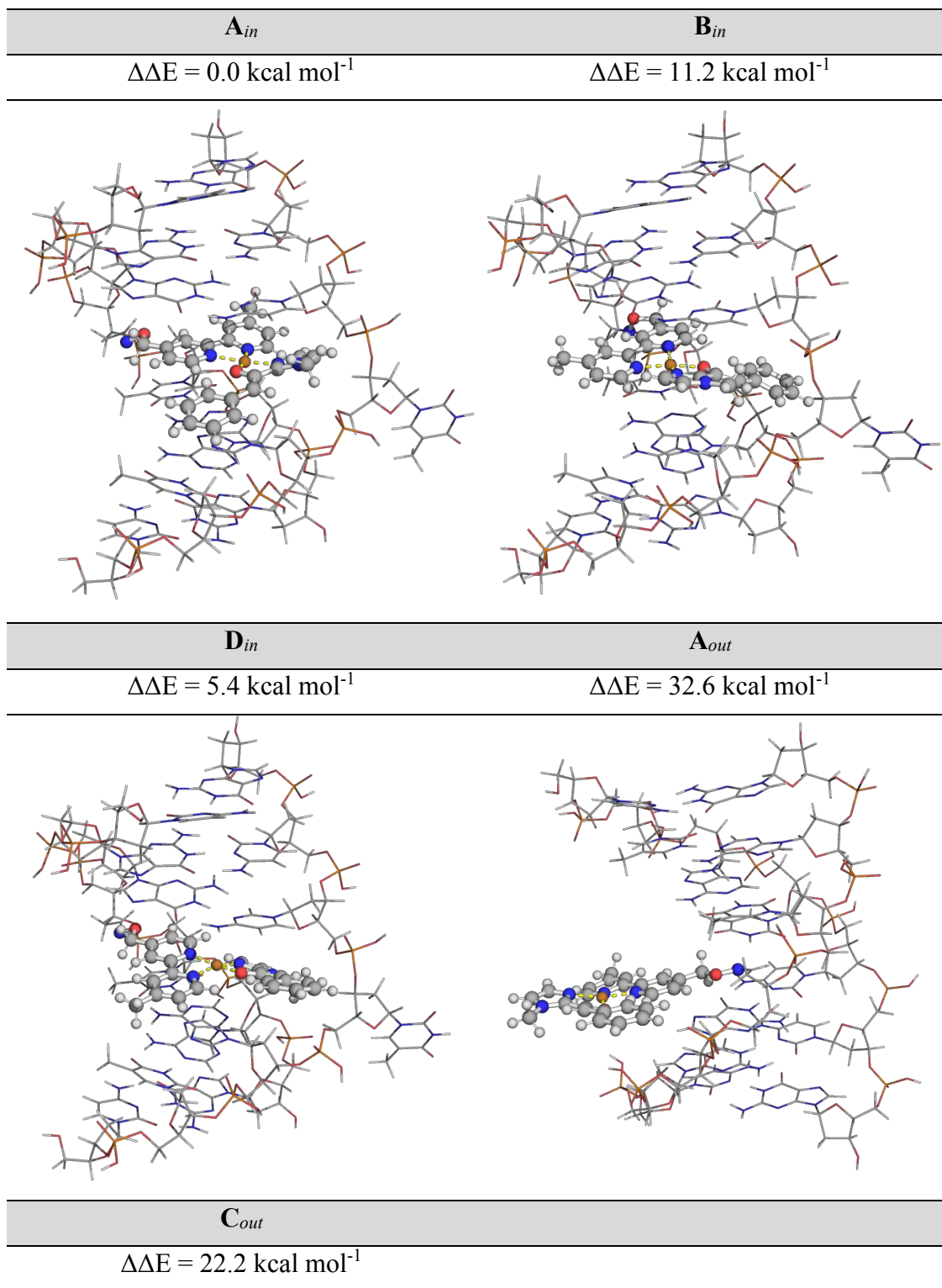


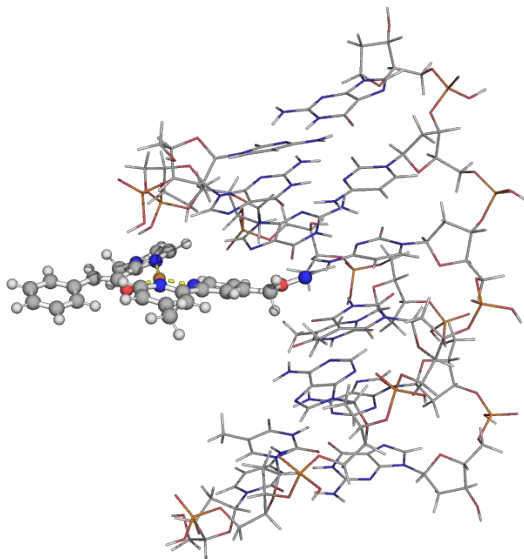
Supplementary Figure 3. Naming conventions for computational model structures.

Fluorination reaction

Unbound states

The GFN2-xTB-optimized structures of the DNA model system used for fluorination reaction are shown in **Supplementary Figure 4**. The energies of the structures with the catalyst system in the “out states”, where the opposite base remain inside the duplex, and in the “in states”, where the catalyst system tucks in between DNA base pairs and the opposite base is flipped out, were compared. It was found that the “in states” are lower in energy than the “out states”, thus more thermodynamically stable. This may be due to the more favorable π - π stacking interactions in the “in states”. In particular, structure **A**_{in} is the most stable and is taken as the zero-energy reference.





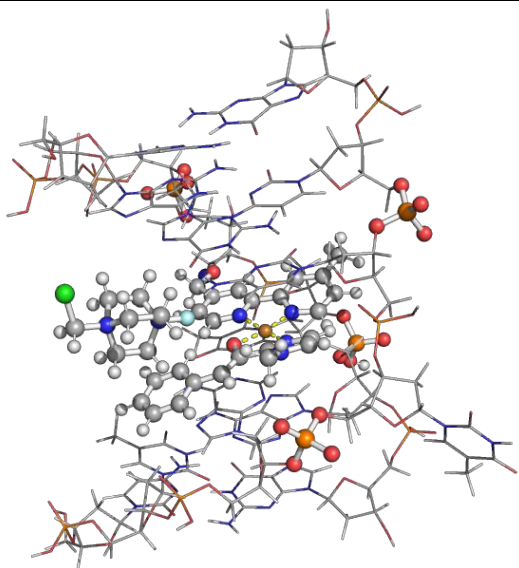
Supplementary Figure 4. GFN2-xTB-optimized structures of the DNA model system used for fluorination reaction. Energy values are given in kcal mol⁻¹ and taken relative to the most stable complex.

Bound states

The GFN2-xTB-optimized structures of the structures where the Selectfluor cation binds are shown in **Supplementary Figure 5**. The most stably bound species is **B_{in}_F_{re}**, which gives the right enantioselectivity outcome in the fluorination products. We observed that the Selectfluor cation can approach the substrate in the minor groove and interact with the phosphate groups 5 and 15 through ionic interactions. Different protonation states of the phosphates were considered (**B_{in}_F_{re}** where phosphates 3, 5, 15 are deprotonated, and **B_{in}_F_{re}_P2** where phosphates 5, 13, 15 are deprotonated) and the most stable one was located. Note, that we have deprotonated both phosphates 5 and 15 in both cases, as these two are important to form ionic interactions with the positively charged Selectfluor cation.

The complexes where the catalyst is in the “out states” where the Selectfluor cation binds were also considered. These species **A_{out}_F_{si/re}** and **C_{out}_F_{si/re}** have higher energies than the complexes where the catalyst is in the “in states” (**Supplementary Figure 3**), similar to the scenario observed for the unbound states (**Supplementary Figure 4**).

A_{in}_F_{si}
$\Delta\Delta E = 1.2 \text{ kcal mol}^{-1}$

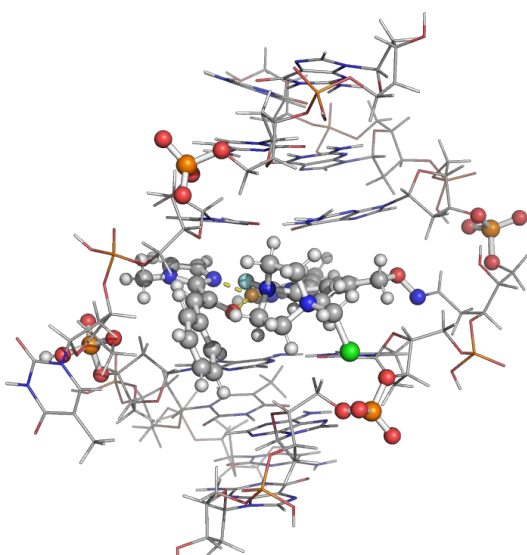
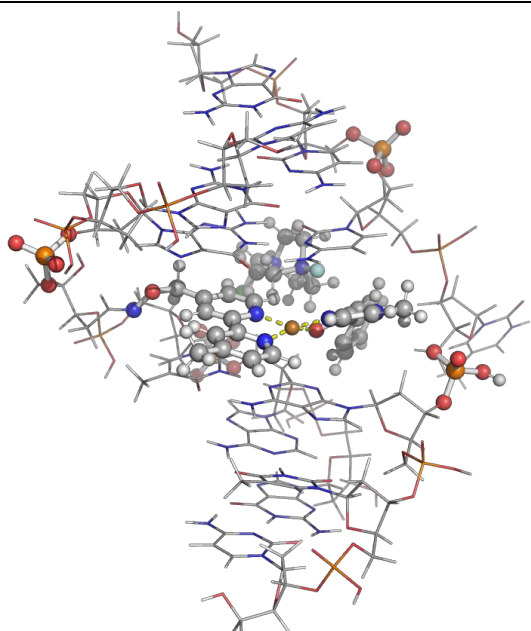


B_{in}_Fre (front view)

B_{in}_Fre (back view)

$\Delta\Delta E = 0.0 \text{ kcal mol}^{-1}$

$\Delta\Delta E = 0.0 \text{ kcal mol}^{-1}$

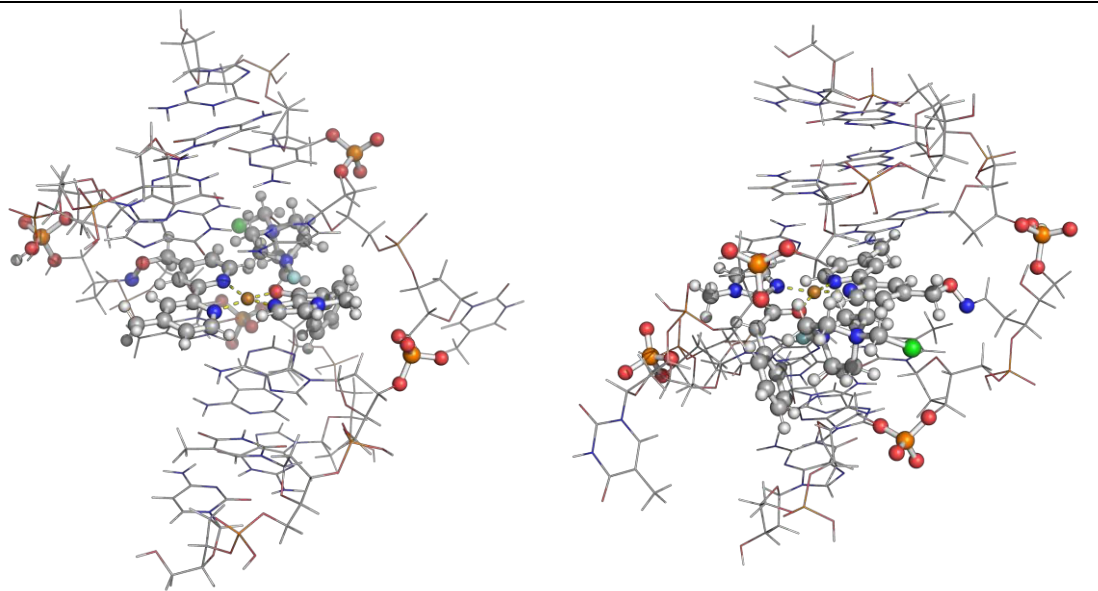


B_{in}_Fre_P2 (front view)

B_{in}_Fre_P2 (back view)

$\Delta\Delta E = 9.7 \text{ kcal mol}^{-1}$

$\Delta\Delta E = 9.7 \text{ kcal mol}^{-1}$

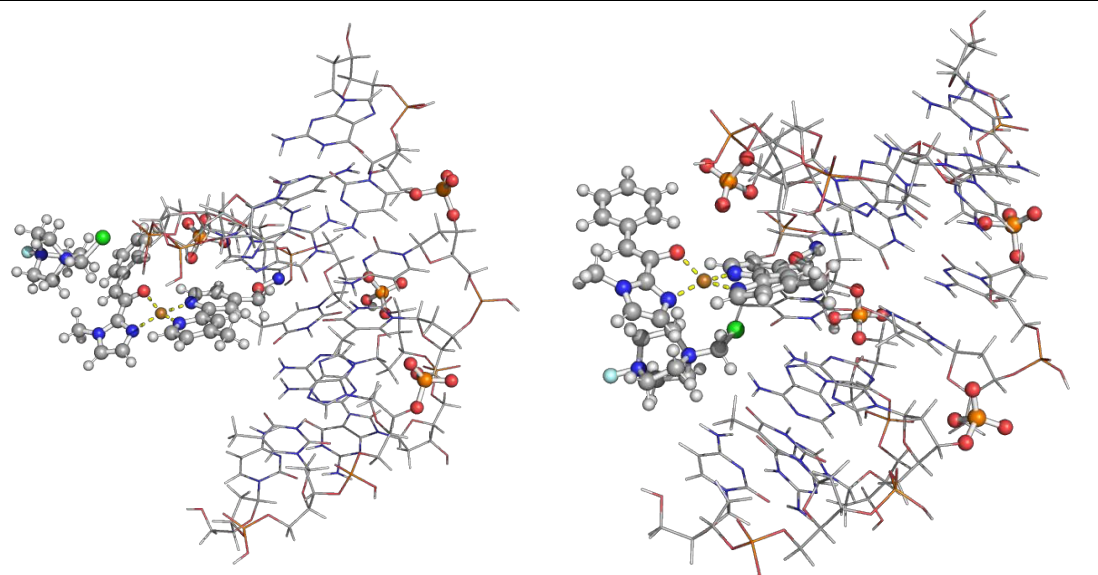


A_{out}_F_{si}

$$\Delta\Delta E = 10.4 \text{ kcal mol}^{-1}$$

A_{out}_F_{re}

$$\Delta\Delta E = 20.0 \text{ kcal mol}^{-1}$$

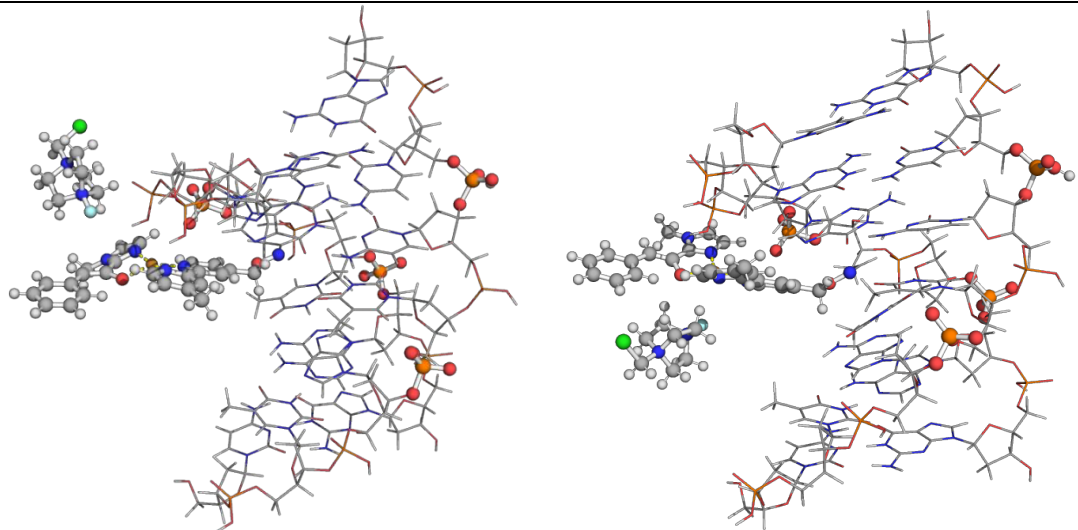


C_{out}_F_{re}

$$\Delta\Delta E = 7.7 \text{ kcal mol}^{-1}$$

C_{out}_F_{si}

$$\Delta\Delta E = 25.6 \text{ kcal mol}^{-1}$$



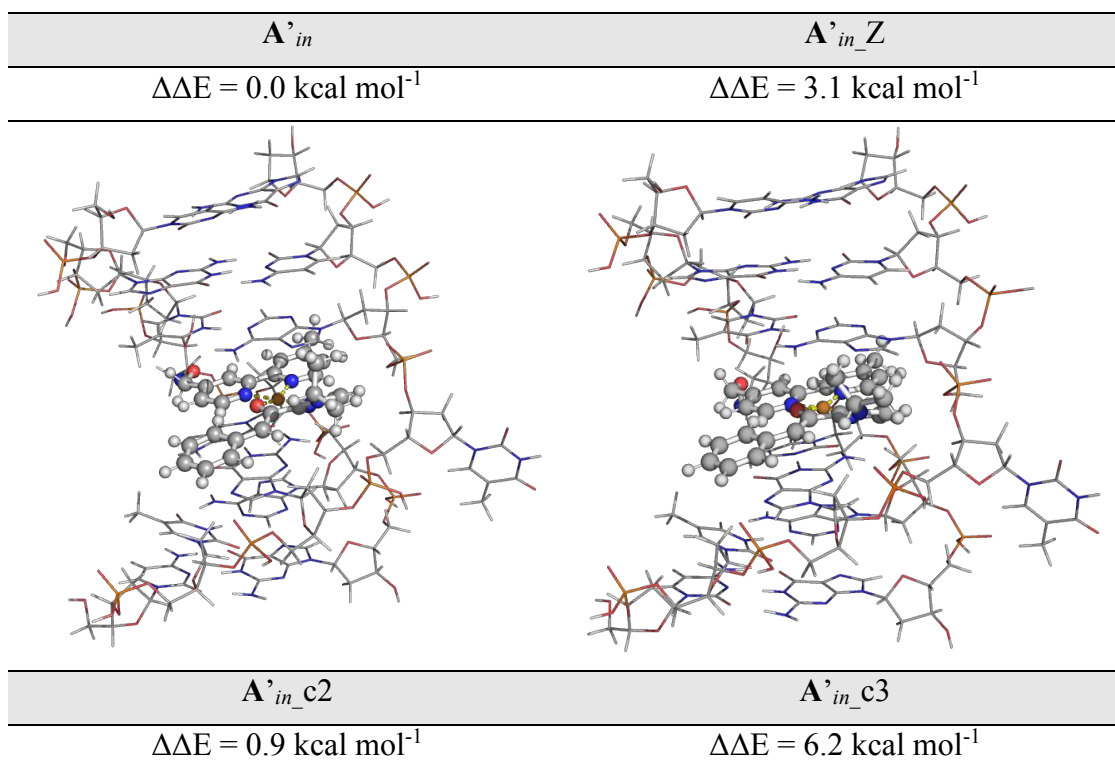
Supplementary Figure 5. GFN2-xTB-optimized fluorination reaction with Selectfluor binding. Energy values are given in kcal mol⁻¹ and taken relative to the most stable complex.

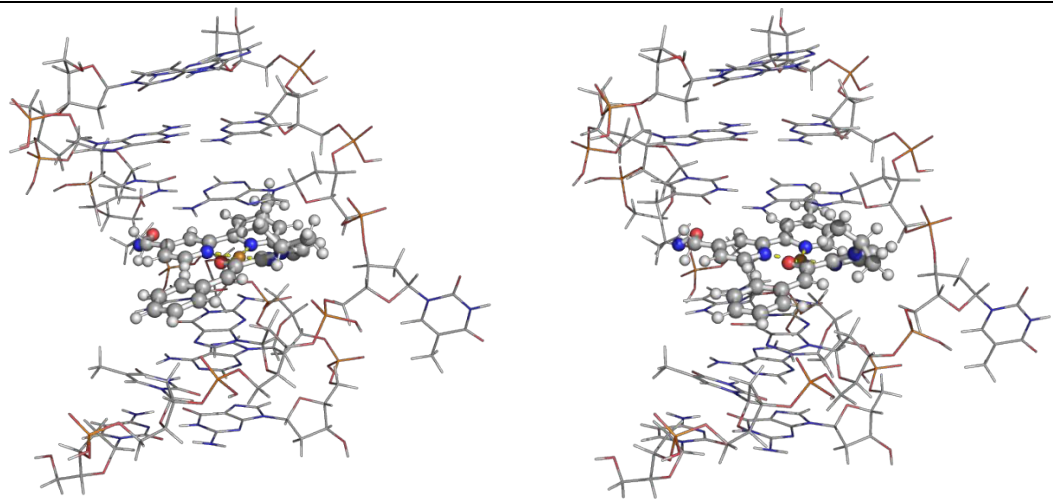
Mannich reaction

Unbound states

The mechanistic basis for these sequence-dependent effects on reactivity and selectivity in the Mannich reaction was studied computationally. The GFN2-xTB-optimized structures of the DNA model used for Mannich reaction were shown in **Supplementary Figure 6**.

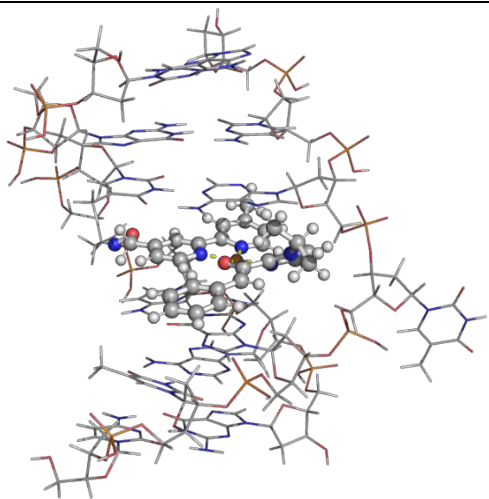
For the A' “in states”, the conformers of the *iPr*-group on the Cu-bound substrate were considered (**A'**_{in}, **A'**_{in_c2} and **A'**_{in_c3}) and the lowest one (**A'**_{in}) is used as the zero-energy reference. We also found that the structure with the oxime in Z configuration (**A'**_{in_Z}) is higher in energy, by 3.1 kcal mol⁻¹, than the structure with oxime in E configuration (**A'**_{in}), as expected. The “out states” are again higher in energies than the “in states”.





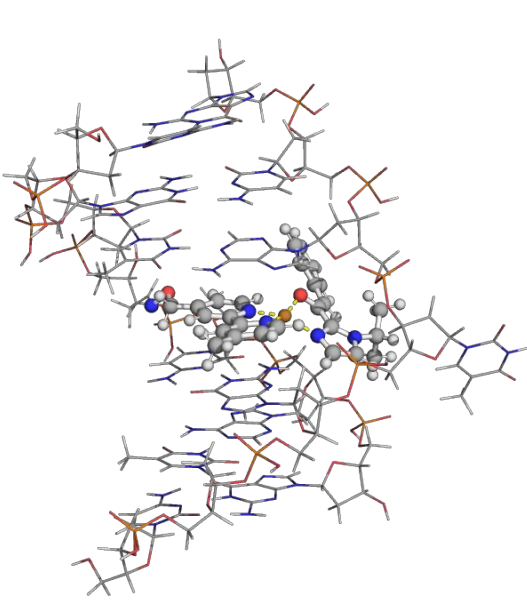
B' *in*

$$\Delta\Delta E = 18.3 \text{ kcal mol}^{-1}$$



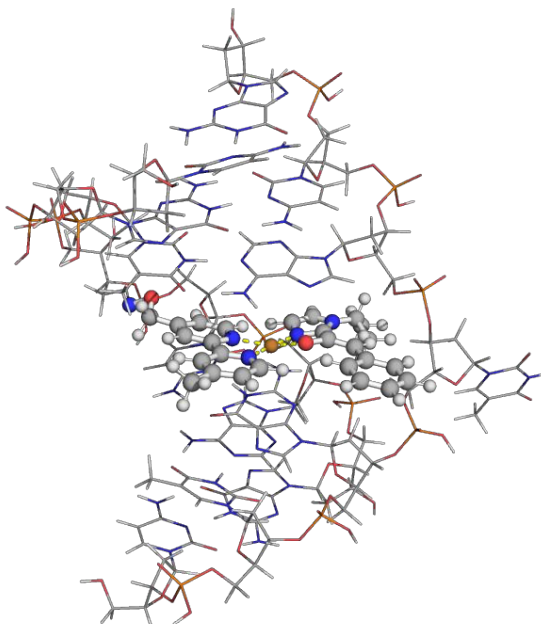
D' *in*

$$\Delta\Delta E = 0.9 \text{ kcal mol}^{-1}$$



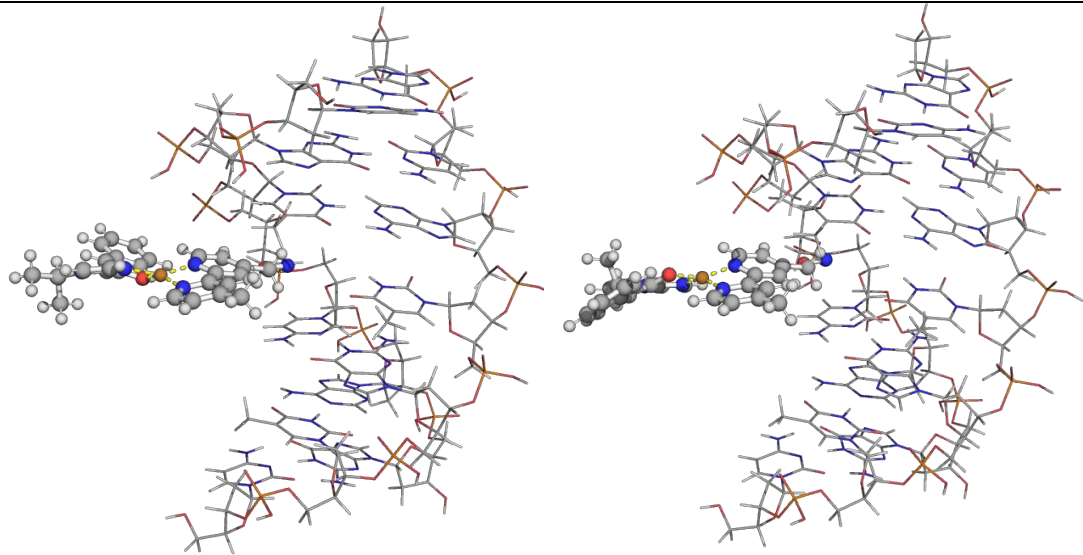
A' *out*

$$\Delta\Delta E = 27.3 \text{ kcal mol}^{-1}$$



C' *out*

$$\Delta\Delta E = 28.8 \text{ kcal mol}^{-1}$$

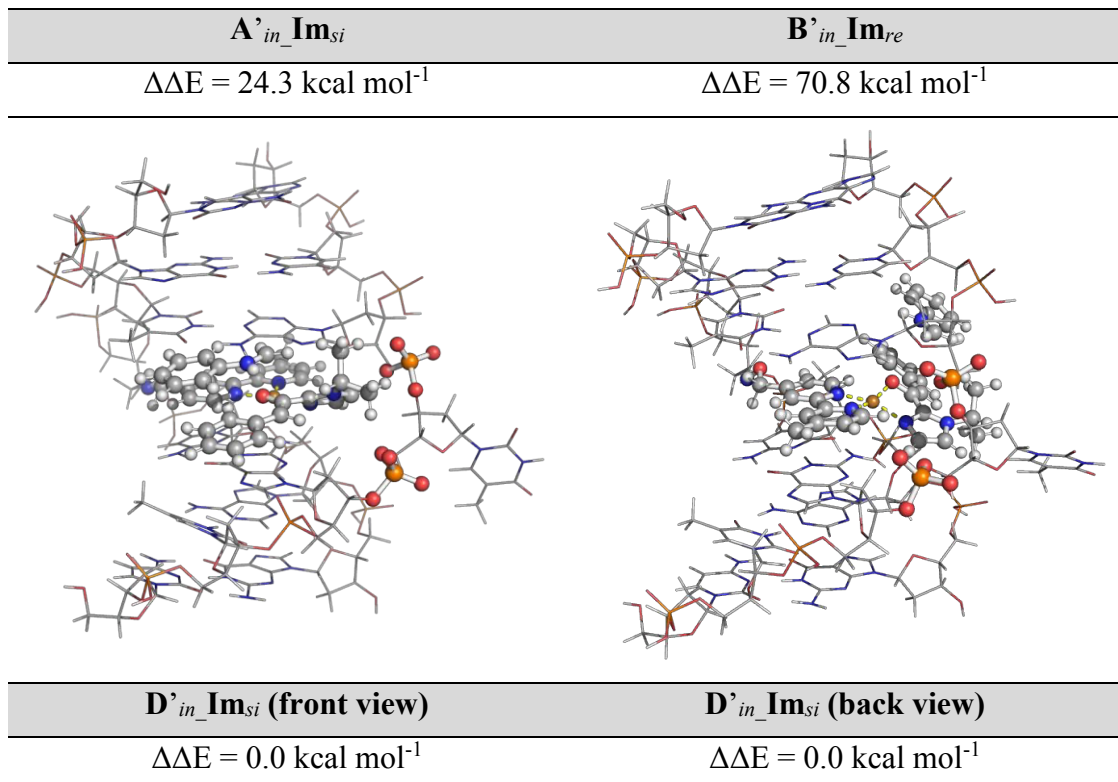


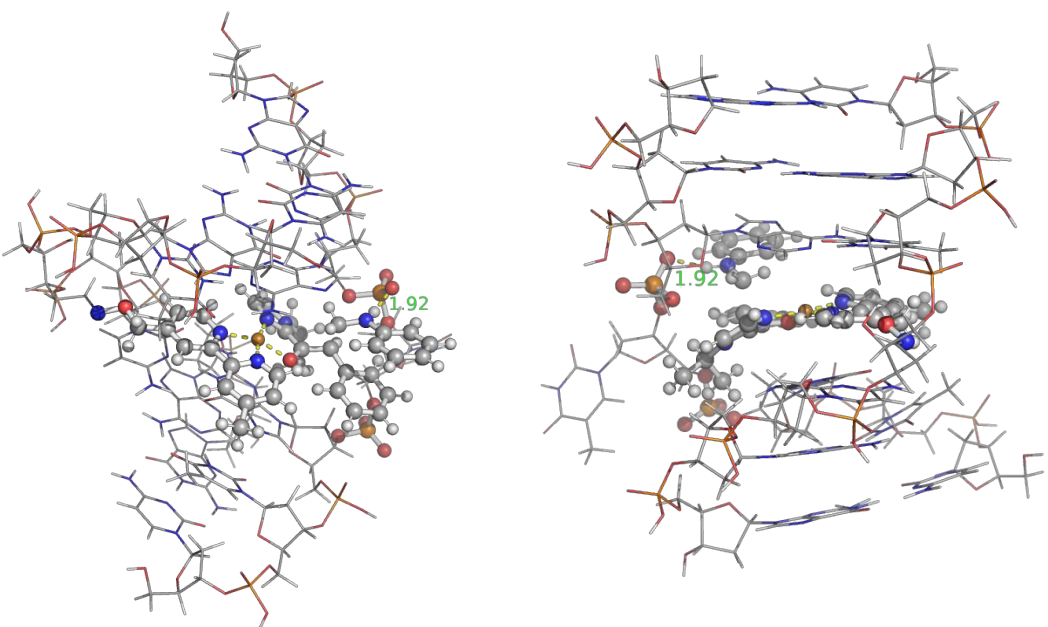
Supplementary Figure 6. GFN2-xTB-optimized structures of the DNA model system used for the Mannich reaction. Energy values are given in kcal mol⁻¹ and taken relative to the most stable complex.

Bound states

The GFN2-xTB-optimized structures of the iminium bound species are shown in **Supplementary Figure 7**. The most stable species is **D' _{in} Im_{si}**, which benefits from favourable hydrogen bonding and electrostatic attraction between the N–H group of the iminium cation and the deprotonated phosphate 14.

The complexes where the catalyst is in the “out states” where the iminium cation binds were also considered. These species **A' _{out} Im_{si/re}** and **C' _{out} Im_{si/re}** have higher energies than the complexes where the catalyst is in the “in states” (**Supplementary Figure 7**), similar to the scenario observed for the unbound states (**Supplementary Figure 6**).



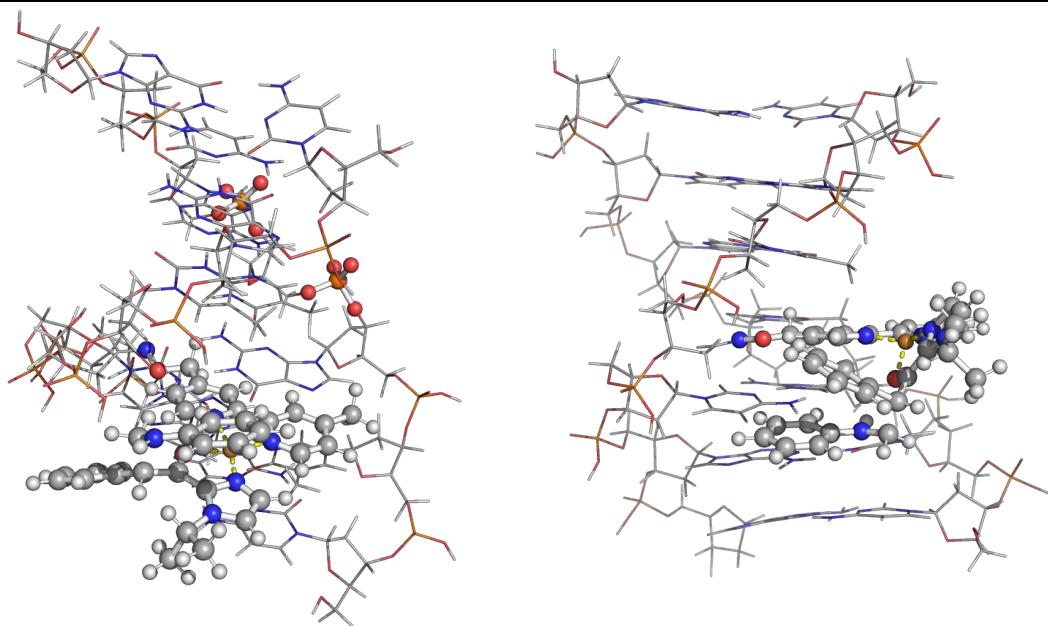


A'_{out} Im_{si}

$\Delta\Delta E = 25.7 \text{ kcal mol}^{-1}$

A'_{out} Im_{re}

$\Delta\Delta E = 39.0 \text{ kcal mol}^{-1}$

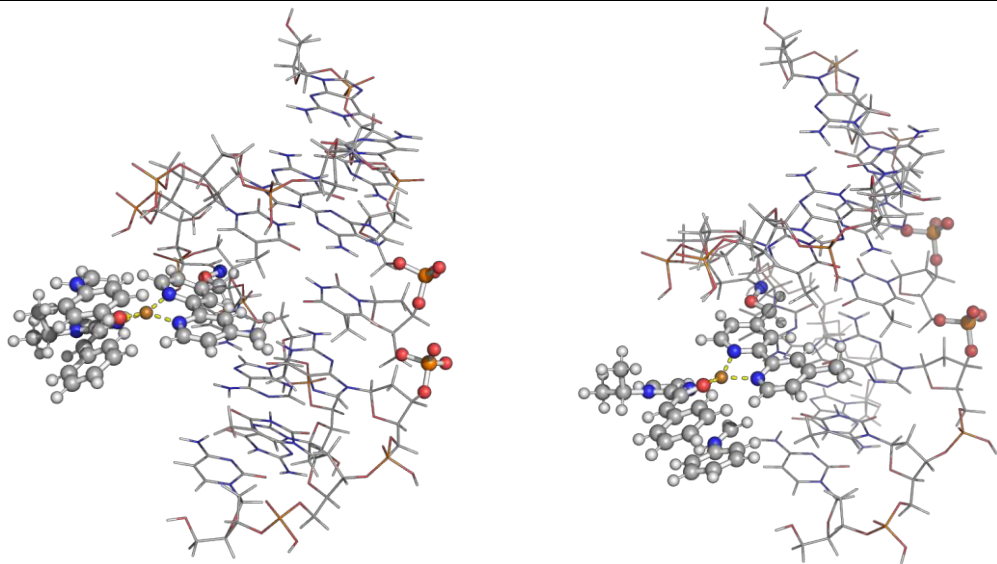


C'_{out} Im_{re}

$\Delta\Delta E = 61.0 \text{ kcal mol}^{-1}$

C'_{out} Im_{si}

$\Delta\Delta E = 53.5 \text{ kcal mol}^{-1}$



Supplementary Figure 7. GFN2-xTB-optimized Mannich reaction model system with iminium binding. Energy values are given in kcal mol⁻¹ and taken relative to the most stable complex.

xTB-optimized structures

Geometries of all xTB-optimized structures (in .xyz format) are included in a separate folder named *xTB_optimized_structures* with an associated *readme.txt* file. All these data have been uploaded to zenodo.org at <https://zenodo.org/records/14043521>, with DOI: [10.5281/zenodo.14043521](https://doi.org/10.5281/zenodo.14043521).

Supplementary References

- (1) Wang, Y. M.; Wu, J.; Hoong, C.; Rauniar, V.; Toste, F. D. Enantioselective Halocyclization Using Reagents Tailored for Chiral Anion Phase-transfer Catalysis. *J. Am. Chem. Soc.*, **2012**, *134*, 12928–12931.
- (2) Sheng, J.; Li, Z.; Koh, K. K. Y.; Shi, Q.; Foo, A.; Tan, P. M. L.; Kha, T.-K.; Wang, X.; Fang, L.; Zhu, R.-Y. Merging DNA Repair with Bioorthogonal Conjugation Enables Accessible and Versatile Asymmetric DNA Catalysis. *J. Am. Chem. Soc.* **2024**, *146*, 16531–16539.
- (3) Bannwarth, C.; Ehler, S.; Grimme, S. GFN2-XTB - An Accurate and Broadly Parametrized Self-Consistent Tight-Binding Quantum Chemical Method with Multipole Electrostatics and Density-Dependent Dispersion Contributions. *J. Chem. Theory Comput.* **2019**, *15* (3), 1652–1671.
- (4) Grimme, S.; Bannwarth, C.; Shushkov, P. A Robust and Accurate Tight-Binding Quantum Chemical Method for Structures, Vibrational Frequencies, and Noncovalent Interactions of Large Molecular Systems Parametrized for All Spd-Block Elements ($Z = 1\text{--}86$). *J. Chem. Theory Comput.* **2017**, *13* (5), 1989–2009.
- (5) Bannwarth, C.; Caldeweyher, E.; Ehler, S.; Hansen, A.; Pracht, P.; Seibert, J.; Spicher, S.; Grimme, S. Extended Tight-Binding Quantum Chemistry Methods. *Wiley Interdiscip. Rev. Comput. Mol. Sci.* **2021**, *11* (2), e1493.
- (6) Frisch, M. J. ; Trucks, G. W. ; Schlegel, H. B. ; Scuseria, G. E. ; Robb, M. A. ; Cheeseman, J. R. ; Scalmani, G. ; Barone, V. ; Petersson, G. A. ; Nakatsuji, H. ; et al. Gaussian 16, Revision B.01. 2016.
- (7) Becke, A. D. Density-Functional Thermochemistry. III. The Role of Exact Exchange. *J. Chem. Phys.* **1993**, *98* (7), 5648–5652.
- (8) Perdew, J. P. Density-Functional Approximation for the Correlation Energy of the Inhomogeneous Electron Gas. *Phys. Rev. B* **1986**, *33* (12), 8822–8824.
- (9) Grimme, S.; Antony, J.; Ehrlich, S.; Krieg, H. A Consistent and Accurate Ab Initio Parametrization of Density Functional Dispersion Correction (DFT-D) for the 94 Elements H-Pu. *J. Chem. Phys.* **2010**, *132* (15), 154104.
- (10) Becke, A. D.; Johnson, E. R. Exchange-Hole Dipole Moment and the Dispersion Interaction. *J. Chem. Phys.* **2005**, *122* (15).
- (11) Johnson, E. R.; Becke, A. D. A Post-Hartree-Fock Model of Intermolecular Interactions. *J. Chem. Phys.* **2005**, *123* (2).
- (12) Johnson, E. R.; Becke, A. D. A Post-Hartree-Fock Model of Intermolecular Interactions: Inclusion of Higher-Order Corrections. *J. Chem. Phys.* **2006**, *124* (17).
- (13) Becke, A. D.; Johnson, E. R. A Density-Functional Model of the Dispersion Interaction. *J. Chem. Phys.* **2005**, *123* (15).
- (14) Ditchfield, R.; Hehre, W. J.; Pople, J. A. Self-Consistent Molecular-Orbital Methods. IX. An Extended Gaussian-Type Basis for Molecular-Orbital Studies of Organic Molecules. *J. Chem. Phys.* **2004**, *54* (2), 724–728.
- (15) Grimme, S. Density Functional Theory with London Dispersion Corrections. *Wiley Interdiscip. Rev. Comput. Mol. Sci.* **2011**, *1* (2), 211–228.
- (16) Burns, L. A.; Vázquez-Mayagoitia, Á.; Sumpter, B. G.; Sherrill, C. D. Density-Functional Approaches to Noncovalent Interactions: A Comparison of Dispersion Corrections (DFT-D), Exchange-Hole Dipole Moment (XDM) Theory, and Specialized Functionals. *J. Chem. Phys.* **2011**, *134* (8).
- (17) Dilabio, G. A.; Koleini, M. Dispersion-Correcting Potentials Can Significantly Improve the Bond

- Dissociation Enthalpies and Noncovalent Binding Energies Predicted by Density-Functional Theory. *J. Chem. Phys.* **2014**, *140* (18).
- (18) Cohen, A. J.; Mori-Sánchez, P.; Yang, W. Challenges for Density Functional Theory. *Chem. Rev.* **2012**, *112* (1), 289–320.
 - (19) Marenich, A. V.; Cramer, C. J.; Truhlar, D. G. Universal Solvation Model Based on Solute Electron Density and on a Continuum Model of the Solvent Defined by the Bulk Dielectric Constant and Atomic Surface Tensions. *J. Phys. Chem. B* **2009**, *113* (18), 6378–6396.
 - (20) Schrödinger, L. *The PyMOL Molecular Graphics Development Component, Version 1.8*; 2015.
 - (21) Xu, G.; Liang, H.; Fang, J.; Jia, Z.; Chen, J.; Xu, P. Catalytic Enantioselective α -Fluorination of 2-Acyl Imidazoles via Iridium Complexes. *Chem. Asian J.* **2016**, *11*, 3355–3358.
 - (22) Gong, J.; Li, S.; Qurban, S.; Kang, Q. Enantioselective Mannich Reaction Employing 1,3,5-Triaryl-1,3,5-triazinanes Catalyzed by Chiral-at-Metal Rhodium Complexes. *Eur. J. Org. Chem.* **2017**, 3584–3593.

Full reference for Gaussian software:

Gaussian 16, Revision B.01, Frisch, M. J.; Trucks, G. W.; Schlegel, H. B.; Scuseria, G. E.; Robb, M. A.; Cheeseman, J. R.; Scalmani, G.; Barone, V.; Mennucci, B.; Petersson, G. A.; Nakatsuji, H.; Caricato, M.; Li, X.; Hratchian, H. P.; Izmaylov, A. F.; Bloino, J.; Zheng, G.; Sonnenberg, J. L.; Hada, M.; Ehara, M.; Toyota, K.; Fukuda, R.; Hasegawa, J.; Ishida, M.; Nakajima, T.; Honda, Y.; Kitao, O.; Nakai, H.; Vreven, T.; Montgomery Jr., J. A.; Peralta, J. E.; Ogliaro, F.; Bearpark, M.; Heyd, J. J.; Brothers, E.; Kudin, K. N.; Staroverov, V. N.; Kobayashi, R.; Normand, J.; Raghavachari, K.; Rendell, A.; Burant, J. C.; Iyengar, S. S.; Tomasi, J.; Cossi, M.; Rega, N.; Millam, J. M.; Klene, M.; Knox, J. E.; Cross, J. B.; Bakken, V.; Adamo, C.; Jaramillo, J.; Gomperts, R.; Stratmann, R. E.; Yazyev, O.; Austin, A. J.; Cammi, R.; Pomelli, C.; Ochterski, J. W.; Martin, R. L.; Morokuma, K.; Zakrzewski, V. G.; Voth, G. A.; Salvador, P.; Dannenberg, J. J.; Dapprich, S.; Daniels, A. D.; Farkas, Ö.; Foresman, J. B.; Ortiz, J. V.; Cioslowski, J.; Fox, D. J. Gaussian, Inc., Wallingford CT, 2016.